Millennial-scale sea surface temperature changes in the eastern Mediterranean (Nile River Delta region) over the last 27,000 years

Isla S. Castañeda,[1] Enno Schefuß,[2] Jürgen Pätzold,[2,3] Jaap S. Sinninghe Damsté,[1] Syee Weldeab,[4] and Stefan Schouten[1]

Received 28 January 2009; revised 17 August 2009; accepted 7 October 2009; published 10 March 2010.

[1] In this study we utilize two organic geochemical proxies, the $U^{k'}_{37}$ index and TEX_{86}, to examine past sea surface temperatures (SST) from a site located near the Nile River Delta in the eastern Mediterranean (EM) Sea. The $U^{k'}_{37}$ and TEX_{86} records generally are in agreement and indicate SST ranges of 14°C–26°C and 14°C–28°C, respectively, during the last 27 cal ka. During the Holocene, TEX_{86}-based SST estimates are usually higher than $U^{k'}_{37}$-based SST estimates, which is likely due to seasonal differences between the timing of the haptophyte and crenarchaeota blooms in the EM and is related to the onset of the modern flow regime of the Nile River. Both records show that SST varied on centennial to millennial timescales in response to global climate events, i.e., cooling during the Last Glacial Maximum (LGM), Heinrich event 1 (H1), and the Younger Dryas (YD) and warming during the Bølling-Allerød and in the early Holocene during deposition of sapropel S1. The H1 cooling was particularly severe and is marked by a drop in SST of ~4.5°C in comparison to pre-H1 SST, with temperatures >1°C cooler than during the LGM. In contrast to high-latitude and western Mediterranean records, which indicate both an abrupt onset and termination of the YD event, the transition from the YD to the Holocene was much more gradual in the EM.

Citation: Castañeda, I. S., E. Schefuß, J. Pätzold, J. S. Sinninghe Damsté, S. Weldeab, and S. Schouten (2010), Millennial-scale sea surface temperature changes in the eastern Mediterranean (Nile River Delta region) over the last 27,000 years, *Paleoceanography*, *25*, PA1208, doi:10.1029/2009PA001740.

1. Introduction

[2] The paleoclimate of the eastern Mediterranean (EM) is of much interest due its long history of human occupation and therefore many studies have been aimed at reconstructing past sea surface temperatures (SSTs) from this region. However, obtaining accurate SST reconstructions from the EM has proven challenging. Paleotemperature and paleosalinity reconstructions based on planktonic foraminifera are complicated by the lack of modern analogs to compare with fossil assemblages [*Hayes et al.*, 2005], while $\delta^{18}O$ analyses are complicated by large changes in salinity that have occurred due to fluctuations in Nile River discharge. The combination of $\delta^{18}O$ measurements in conjunction with the Mg/Ca ratios of foraminiferal calcite allows for the effects of temperature/ice volume and salinity to be separated. However, Mg/Ca ratios are also influenced by salinity [*Nürnberg et al.*, 1996; *Lea et al.*, 1999; *Kisakürek et al.*, 2008] and in the EM where salinity is unusually high, abnormally high Mg/Ca ratios have been observed in comparison to calcification temperatures [*Ferguson et al.*, 2008].

[3] Like the inorganic SST proxies, application of organic geochemical SST proxies to the EM has also proven challenging. The $U^{k'}_{37}$ index [*Prahl et al.*, 1988], which is based on the ratio of long-chain diunsaturated and triunsaturated ketones produced by haptophyte algae [*Brassell et al.*, 1986], is generally considered a robust SST proxy because it is mainly influenced by temperature. Therefore, several studies have used the $U^{k'}_{37}$ index to reconstruct past SSTs from the EM [*Emeis et al.*, 2000, 2003; *Essallami et al.*, 2007]. However, due to generally low organic carbon contents (<1%) in nonsapropel intervals [e.g., *Schilman et al.*, 2003], low abundances or the absence of long-chain alkenones in some sedimentary intervals has hampered efforts to obtain continuous and high-resolution SST records from the EM.

[4] An alternative approach to reconstructing past SSTs is application of the more recently developed TEX_{86} proxy [*Schouten et al.*, 2002], which is based on glycerol dialkyl glycerol tetraethers (GDGTs). These compounds are present in the membrane lipids of Marine Group I Crenarchaeota, which are ubiquitous in marine environments. The TEX_{86} SST proxy is based on the relative abundance of several different types of isoprenoidal GDGTs, which are biosynthesized in varying amounts depending on growth temperature [*Schouten et al.*, 2002]. Like the $U^{k'}_{37}$ index, the

[1]Department of Marine Organic Biogeochemistry, Royal Netherlands Institute for Sea Research, Texel, Netherlands.
[2]MARUM, University of Bremen, Bremen, Germany.
[3]Faculty of Geosciences, University of Bremen, Bremen, Germany.
[4]Department of Earth Science, University of California, Santa Barbara, California, USA.

0883-8305/10/2009PA001740$12.00

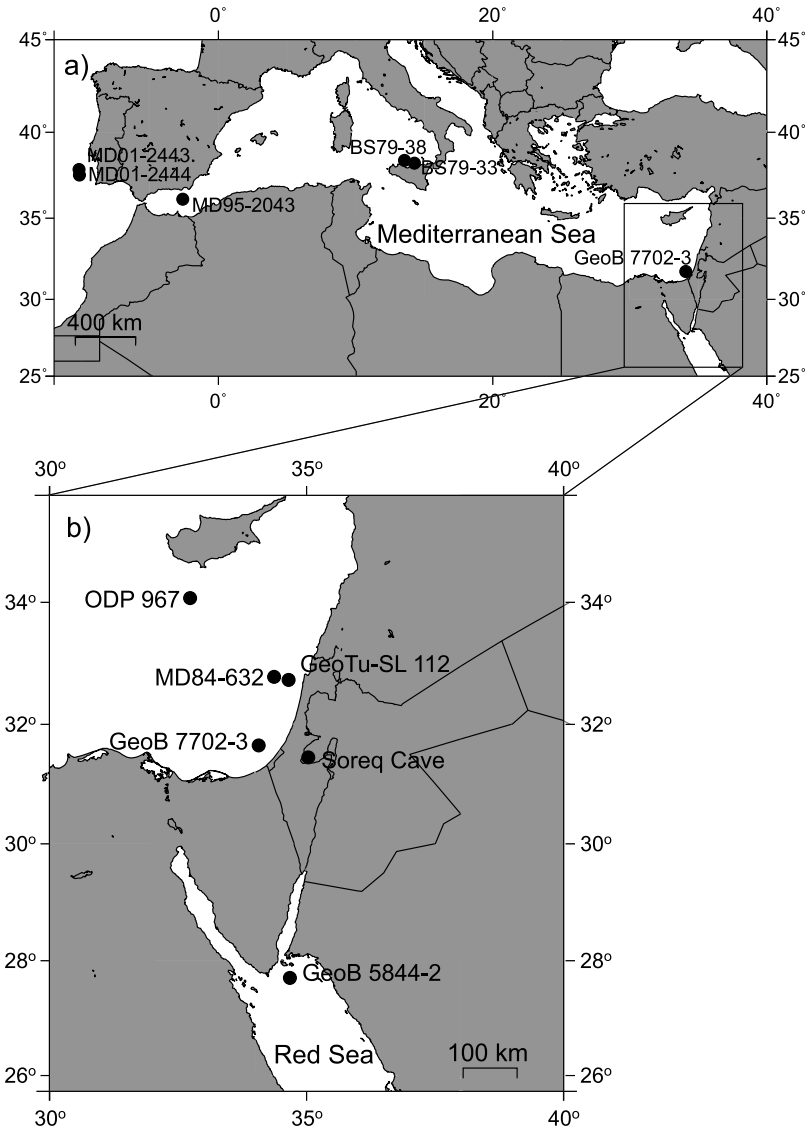

Figure 1. Location of core GeoB 7702-3 in the Mediterranean Sea. (a) Expanded map of the Mediterranean region showing the location of several central and western Mediterranean climate records including MD01-2243 and MD01-2244 [*Martrat et al.*, 2007], MD95-2043 [*Cacho et al.*, 1999, 2001], and BS79-33 and BS79-38 [*Cacho et al.*, 2001]. (b) Detailed map of the eastern Mediterranean showing the location of core GeoB 7702-3. Locations of other climate records are shown for comparison including ODP site 967 [*Emeis et al.*, 2000], MD84-632 [*Essallami et al.*, 2007], GeoTu-SL112 [*Hamann et al.*, 2008], Soreq Cave in Israel [*Bar-Matthews et al.*, 1999, 2003], and Red Sea core GeoB 5844-2 [*Arz et al.*, 2003].

TEX_{86} paleothermometer has the advantage that it does not seem to be influenced by changes in salinity [*Wuchter et al.*, 2004]. TEX_{86} from the EM has been only previously examined in Pliocene sapropels [*Menzel et al.*, 2006] but not in Quaternary sediments.

[5] Here, we examine both $U^{k'}_{37}$ and TEX_{86} from a sediment core collected from near the Nile River Delta in order to examine the SST history of the EM during the last 27 cal ka. To date, relatively few studies have applied both $U^{k'}_{37}$ and TEX_{86} to the same sediments [e.g., *Huguet et al.*, 2006; *Lee et al.*, 2008; *Shah et al.*, 2008; *Kim et al.*, 2009a, 2009b] but this approach is advantageous because it can provide insight into other environmental factors that may influence each proxy.

2. Study Location

[6] Gravity core GeoB 7702-3 (31°39.1′N, 34°04.4′E; 562 m water depth; 592 cm sediment recovery) was collected from the continental slope off Israel aboard a cruise of the R/V *Meteor* in 2002 [*Pätzold et al.*, 2003] (Figure 1). Levantine Surface Water (LSW) is the surface water mass

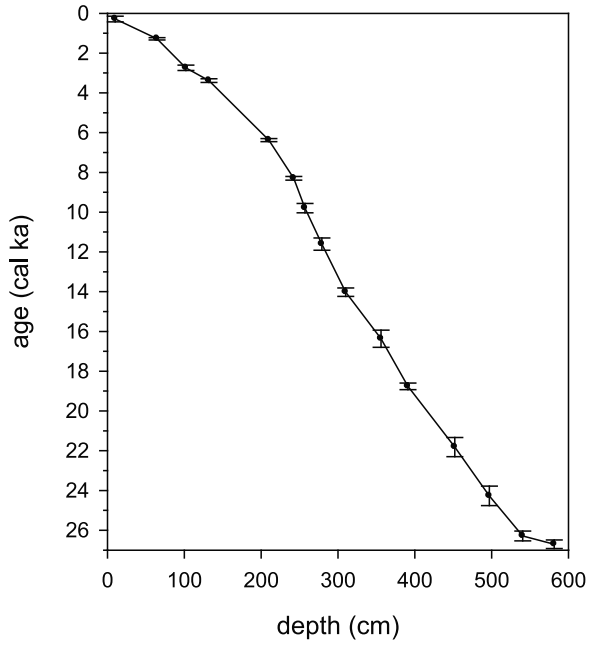

Figure 2. Age-depth model for core GeoB 7702-3 (see also Table 1).

present off the Israeli coast, which extends from 0 to 100 m and ranges in temperature from 17°C in the winter to 27.5°C in the summer [*Marullo et al.*, 1999]. The surface currents flow in an anticlockwise direction around the EM basin and sediment from the Nile River, which is the main sediment supply to the EM, is transported eastward to the coring site [*Weldeab et al.*, 2002]. Aeolian sediment supply is also significant and in some regions of the EM it may be equal to, or even exceed, riverine sediment supply [*Guerzoni et al.*, 1999]. The main source of this dust is from the Sahara with transport to the EM from North Africa mainly occurring during spring, associated with eastward moving frontal low-pressure systems [*Goudie and Middleton*, 2001]. Strong easterly winds over Israel can transport dust from the Middle East to the EM, and typically occur during autumn [*Kubilay et al.*, 2000].

[7] The Nile River consists of two main branches, the Blue Nile (sourced at Lake Tana, Ethiopia) and the White Nile (sourced at Lake Victoria in equatorial Africa). The Blue Nile provides most of the water and particulate matter whereas the White Nile provides the base flow for the Nile River [*Adamson et al.*, 1980]. Prior to the construction of the Aswan Dam on the Nile River in 1965, seasonal flood discharge provided the main supply of terrestrial nutrients to the EM [*Schilman et al.*, 2001, and references therein]. Nutrients and dissolved organic carbon from the Nile River were transported eastward along the coast of Israel causing increased productivity [*Rossignol-Strick et al.*, 1982; *Wadie*, 1984]. Sedimentary data suggests that a similar relationship existed throughout the past 1400 years, and also likely prior to this time, with increased productivity in the EM noted during times of increased monsoonal rainfall in the Nile headwaters [*Schilman et al.*, 2001].

3. Methods

3.1. Chronology

[8] The chronology of GeoB 7702-3 is based on 15 AMS dates (Figure 2), which were analyzed at the Leibniz Laboratory for Radiometric Dating and Stable Isotope Research (University of Kiel, Germany), using monospecific (*Globigerinoides ruber*) and mixed planktonic foraminifers (Table 1). After wet sieving, approximately 10 mg of foraminiferal shells (250–400 μm) were hand picked, cleaned with hydrogen peroxide (H_2O_2) and converted to carbon dioxide (CO_2) by dissolution in hot 100% phosphoric acid. The resulting CO_2 gas was purified and reduced to graphite over an iron catalyst in the presence of H_2 (conducted at the University of Bremen, Germany). For conversion of the ^{14}C dates to calendar ages, the CALIB 5.01 program [*Stuiver and Reimer*, 1993] and the Marine04 Data Set [*Hughen et al.*, 2004] were used with an average Atlantic reservoir age of ~400 years. For ^{14}C ages older than 21,000 years we use the calibration curve and data set of *Fairbanks et al.* [2005] (Table 1). The complete data set covers the past 26.7 thousand calendar years (cal ka).

Table 1. List of Radiocarbon Dates for GeoB 7702-3

Depth (cm)	Laboratory Code	Material	^{14}C Age	Error	2σ Ranges (years B.P.)	Average Calendar Age (B.P.)
10	KIA25649	*G. ruber* and *O. universa*	245	±30	142–425	283.5
64.5	KIA25648	*G. ruber* and *G. sacculifer*	1,725	±25	1,223–1,337	1,280.0
102	KIA24619	*G. ruber*	2,965	±55	2,605–2,876	2,740.5
132	KIA24617	*G. ruber*	3,500	±35	3,292–3,477	3,384.5
210	KIA24616	*G. ruber*	5,600	±40	6,299–6,452	6,375.5
242.5	KIA25646	*G. ruber* and *G. sacculifer*	7,845	±40	8,201–8,390	8,295.5
257	KIA24613	*G. ruber*	9,070	±60	9,558–10,035	9,796.5
279	KIA24612	mixed planktonic foraminifers	10,470	±70	11,301–11,912	11,606.5
310	KIA24611	mixed planktonic foraminifers	12,580	±80	13,813–14,235	14,024.0
356	KIA24609	*G. ruber*	14,130	±100	15,937–16,800	16,368.5
391	KIA24608	*G. ruber*	15,830	±120	18,593–18,927	18,760.0
452	KIA25652	*G. ruber*	18,810	±150	21,334–22,297	21,815.5
497	KIA24605	*G. ruber*	20,660	±180	23,782–24,762	24,272.0
540.5	KIA24604	*G. ruber*	21,840	±220	uncertainty ±247	26,290.0
581.5	KIA25653	mixed planktonic foraminifers	22,230	±190	uncertainty ±215	26,702.0

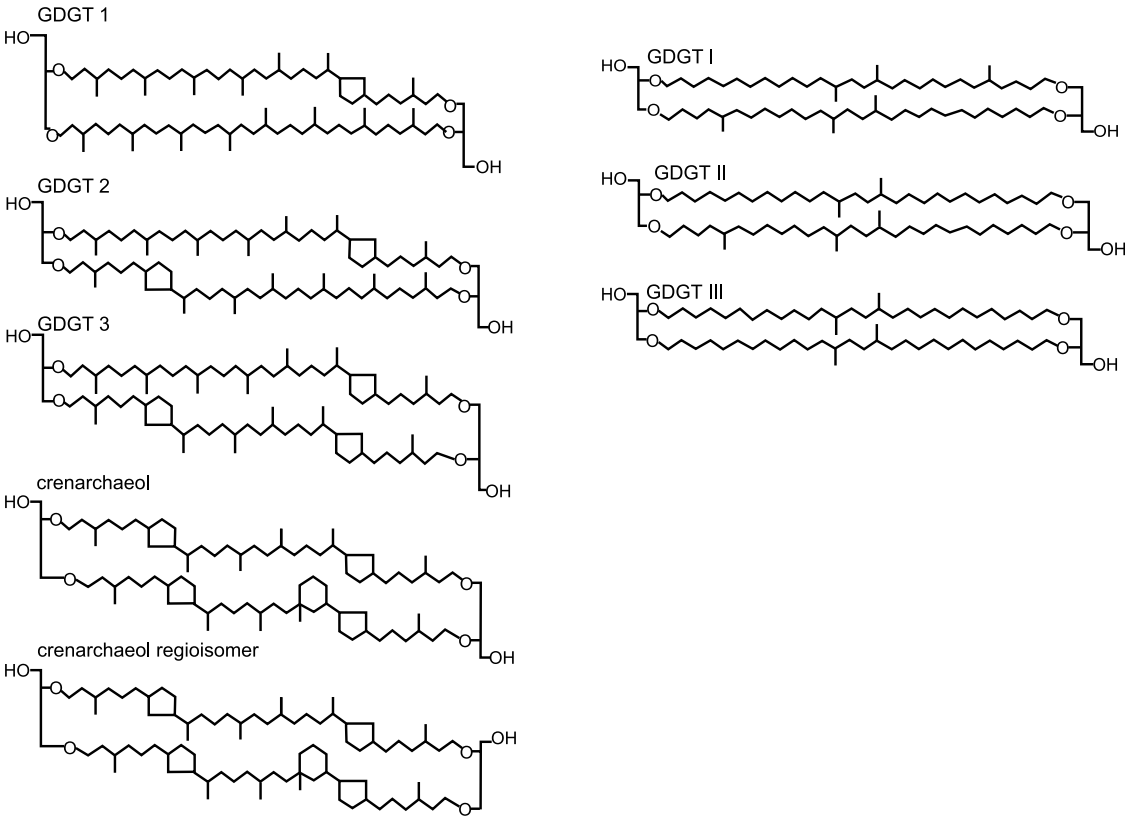

Figure 3. Molecular structures of glycerol dialkyl glycerol tetraethers (GDGTs) used for calculation of the TEX_{86} [*Schouten et al.*, 2002] and BIT indices [*Hopmans et al.*, 2004].

3.2. Extraction and Fractionation of Organic Compounds

[9] Core GeoB 7702-3 was sampled at 5 cm intervals. Freeze-dried sediment samples were extracted with a DIONEX Accelerated Solvent Extractor (ASE 200) using a solvent mixture of 9:1 dichloromethane (DCM) to methanol (MeOH). After extraction, known amounts of three internal standards were added to the total lipid extract (TLE); squalene, 10-nonadecanone (C_{19} ketone), and a C_{46} GDGT. The TLE was next separated into apolar, ketone and polar fractions via alumina pipette column chromatography using solvent mixtures of 9:1 (vol:vol) hexane/DCM, 1:1 (vol:vol) hexane/DCM, and 1:1 (vol:vol) DCM/MeOH, respectively. After column chromatography, the squalene eluted in the apolar fraction, the C_{19} ketone in the ketone fraction and the C_{46} GDGT in the polar fraction.

3.3. $U^{k'}_{37}$ Analysis

[10] Molecular identification of the $C_{37:2}$ and $C_{37:3}$ alkenones was performed on a Thermo Finnigan Trace Gas Chromatograph (GC) Ultra coupled to Thermo Finnigan DSQ mass spectrometer (MS). A CP Sil-5 fused silica capillary column was used (25 m × 0.32 mm; film thickness = 0.12 μm) with helium as the carrier gas. The column was directly inserted into the electron impact ion source of the DSQ quadrupole mass spectrometer. Mass scans were made in the range of m/z = 50–800 with 3 scans per second and an ionization energy of 70 eV. The temperature program initiated at 70°C, increased first at a rate of 20°C per minute to 130°C, and next at a rate of 4°C min to the final temperature of 320°C, which was held for 10 min.

[11] For quantification of alkenones, samples were analyzed on an HP 6890 GC using a 50 m CP Sil-5 column (0.32 mm diameter, film thickness of 0.12 μm) and helium as the carrier gas. The oven program initiated at 70°C and increased by a rate of 20°C/min to 200°C and next by a rate of 3°C/min until 320°C. The final temperature of 320°C was held for 25 min. Compound concentrations were determined by relating chromatogram peak areas to the concentration of the internal standard.

[12] The $U^{k'}_{37}$ index, defined as $C_{37:2}/(C_{37:2} + C_{37:3})$, was used to estimate SSTs [*Prahl et al.*, 1988]. $U^{k'}_{37}$ values were converted to SSTs using the core top calibration of *Conte et al.* [2006], which includes the data set used in the previously published Mediterranean calibration of *Ternois et al.* [1997]:

$$T°C = -0.957 + 54.293\left(U^{k'}_{37}\right) - 52.894\left(U^{k'}_{37}\right)^2 + 28.321\left(U^{k'}_{37}\right)^3$$

[13] Twenty three samples contained enough alkenones to be run in duplicate or triplicate with a reproducibility of on average ±0.5°C.

3.4. TEX_{86} and the BIT Index

[14] The polar fractions, containing the GDGTs, were ultrasonically dissolved in a mixture of 99:1 (vol:vol) hexane: propanol and filtered through 0.45 μm PFTE filters. GDGTs were analyzed by high pressure liquid chromatography–mass spectrometry (HPLC/MS) following the methods described by *Hopmans et al.* [2000], with minor modifications [*Schouten et al.*, 2007]. Samples were analyzed on an Agilent 1100 series LC/MSD SL with an autoinjector and Chemstation software. A Prevail Cyano column (150 mm × 2.1 mm, 3 μm) was used with 99:1 hexane:propanol (vol:vol) as an eluent. After the first 5 min, the eluent increased by a linear gradient up to 1.8% isopropanol (vol) over the next 45 min at a flow rate of 0.2 mL/min. Scanning was performed in single ion monitoring (SIM) mode to increase sensitivity and reproducibility. The TEX_{86} ratio was calculated following *Schouten et al.* [2002]:

$$TEX_{86} = \frac{[\text{GDGT 2} + \text{GDGT 3} + \text{crenarchaeol regioisomer}]}{[\text{GDGT 1} + \text{GDGT 2} + \text{GDGT 3} + \text{crenarchaeol regioisomer}]}$$

where the GDGTs refer to the structures shown in Figure 3. TEX_{86} values were converted to SSTs using the calibration of *Kim et al.* [2008] where

$$T = -10.78 + 56.2^{*}TEX_{86}$$

[15] The Branched and Isoprenoid Tetraether (BIT) index, a proxy for soil versus marine organic matter input to sediments, was calculated following *Hopmans et al.* [2004]:

$$BIT = \frac{[\text{GDGT I} + \text{GDGT II} + \text{GDGT III}]}{[\text{GDGT I} + \text{GDGT II} + \text{GDGT III} + \text{crenarchaeol}]}$$

where the GDGTs refer to structures shown in Figure 3.

[16] Twenty five of the 115 samples analyzed in this study were run in duplicate for TEX_{86} and the BIT index. For TEX_{86}, the pooled standard deviation of these duplicate runs is better than ±0.02, which corresponds to <1°C using the TEX_{86} calibration of *Kim et al.* [2008]. For the BIT index, the pooled standard deviation of duplicate runs is on average ±0.01.

4. Results and Discussion

4.1. SST Estimates: $U^{k'}_{37}$ and TEX_{86}

[17] In core GeoB 7702-3, SST estimates based on $U^{k'}_{37}$ range from 14°C to 26°C, while SST estimates based on TEX_{86} exhibit a comparable range from 14°C to 28°C (Figure 4). While GDGTs are abundant throughout core GeoB 7702-3, in 56% of the samples long-chain alkenones were either not present or were below the detection limit, and alkenones were absent in all samples older than 24.2 cal ka (Figure 5). Low abundances of alkenones in certain parts of the record may be attributed to a number of ecological factors including changes in nutrient supply, salinity or light limitation [e.g., *Prahl et al.*, 2006; *Versteegh et al.*, 2001], or to changes in lateral transport and preservation [*Mollenhauer et al.*, 2007, 2008]. Nevertheless, despite low abundance of alkenones in parts of the record, the $U^{k'}_{37}$ and TEX_{86} records generally indicate similar overall trends and absolute temperatures (Figure 4). In the early Holocene at ~10 cal ka, significantly warmer TEX_{86} temperatures are noted and this offset is maintained throughout the entire Holocene. The offset between the two records varies from approximately 1°C to 5°C and is the greatest in the early Holocene from ~9–7 cal ka.

[18] A likely explanation for the observed warmer TEX_{86} SSTs in the Holocene compared with $U^{k'}_{37}$ SST records may lie in seasonal differences between the timing of the crenarchaeota and haptophyte blooms in the EM. At present, the annual phytoplankton blooms occurs during the winter (November–March), after deep water mixing occurs and breaks up stratification, and ends upon phosphate depletion [*Krom et al.*, 2003]. In March–April, the water column becomes stratified and a deep chlorophyll maximum forms, which remains throughout the remainder of the year [*Krom et al.*, 2003]. In the EM, maximum coccolith fluxes to sediment traps were observed to occur in the early spring [*Ziveri et al.*, 2000] and $U^{k'}_{37}$ SST estimates of ~19°C have been reported from Mediterranean sediment trap samples [*Ternois et al.*, 1997], representing the winter SST and the season of highest haptophyte production. These observations are further supported by $U^{k'}_{37}$ SSTs of ~19°C in EM surface sediments [*Emeis et al.*, 2000]. Although it was not possible to obtain a $U^{k'}_{37}$ measurement from the uppermost sediment sample, $U^{k'}_{37}$ SSTs of ~23°C–25°C are noted throughout the Holocene. This temperature range is cooler than modern summer SSTs of 27.5°C for the EM but warmer than previously reported spring SSTs of 16.6°C to 20.2°C [*Brasseur et al.*, 1996; *Marullo et al.*, 1999]. Thus, it appears that $U^{k'}_{37}$ at our site may reflect a late spring or early autumn SST.

[19] Although no data is presently available on when the crenarchaeota bloom occurs in the EM, it has been observed that the main crenarchaeota bloom typically does not coincide with the main phytoplankton bloom [*Murray et al.*, 1999; *Wuchter et al.*, 2005]. In GeoB 7702-3, the uppermost sediment sample (5 cm depth; 142 years B.P.) yields a TEX_{86} temperature of 26.4°C, which is in good agreement with summer SST [*Brasseur et al.*, 1996; *Marullo et al.*, 1999]. This is supported by the conclusions of *Menzel et al.* [2006] who reported warmer TEX_{86} SSTs compared with $U^{k'}_{37}$ SSTs in several Pliocene sediment cores from the Mediterranean and suggested that TEX_{86} outside of sapropel layers likely reflects summer SST (TEX_{86} within sapropel layers is discussed in section 4.2.5). We therefore suggest that TEX_{86} in the EM reflects summer SST during the Holocene. During the Late Pleistocene, TEX_{86} may reflect the spring or autumn SST because TEX_{86} SST estimates are in this period similar to that of $U^{k'}_{37}$ SSTs. Alternatively, $U^{k'}_{37}$ may reflect summer SST during the Late Pleistocene.

[20] Before making any paleoclimatic interpretations from the SST records, it is important to consider possible effects of factors other than temperature on the $U^{k'}_{37}$ and TEX_{86} records. For example, while TEX_{86} seems not to be affected

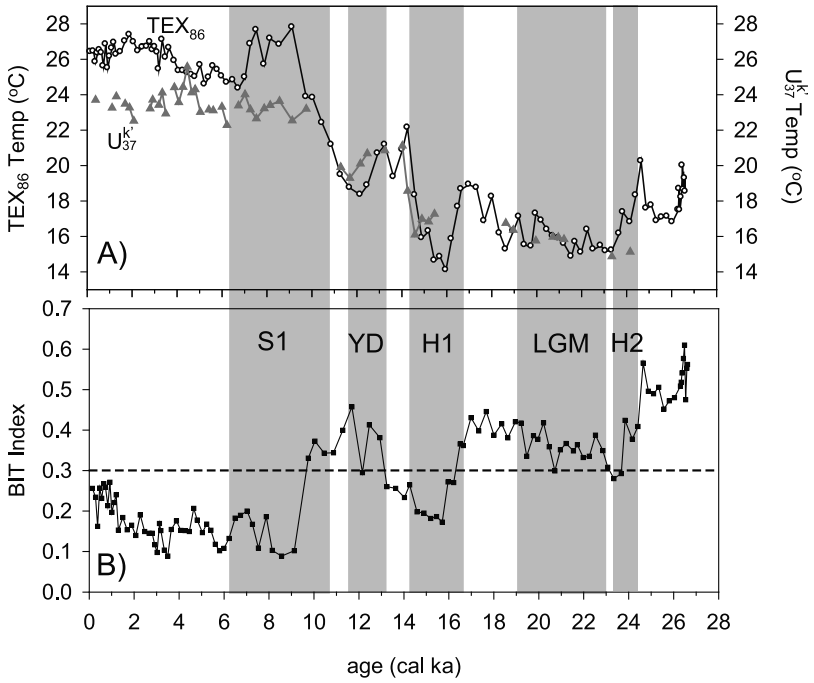

Figure 4. Isoprenoidal GDGT and alkenone-based proxies for core GeoB 7702-3. The intervals of Heinrich event 2 (H2), the Last Glacial Maximum (LGM), Heinrich event 1 (H1), the Younger Dryas (YD), and sapropel S1 (S1) are highlighted. (a) Comparison of TEX_{86} and $U^{k'}_{37}$ reconstructed SSTs. TEX_{86} values are indicated by the open circles, and $U^{k'}_{37}$ values are indicated by the gray triangles. The calibration of *Kim et al.* [2008] was applied for TEX_{86}, while the calibration of *Conte et al.* [2006] was used for $U^{k'}_{37}$. (b) BIT index values. The dashed line at 0.3 is the general boundary above which soil organic matter input may influence the TEX_{86} record [*Weijers et al.*, 2006].

by changes in salinity [*Wuchter et al.*, 2004], it can be influenced by fluvial input of soil-derived isoprenoid GDGTs [*Weijers et al.*, 2006]. The BIT index [*Hopmans et al.*, 2004] provides a method to assess the relative amount of soil organic matter input. In general, TEX_{86} is considered to be applicable in settings where the BIT index is ~<0.3 [*Weijers et al.*, 2006]. BIT values in core GeoB 7702-3 range from a low of 0.09 to a high of 0.61 (Figure 4), and thus parts of the record are characterized by relatively high soil organic matter input, which is not surprising giving the proximity to the mouth of the Nile River. BIT values of >0.3 are noted during the time intervals of 27–16.5 cal ka and from 12.9 to 9.7 cal ka, suggesting increased inputs of soil organic matter at these times. However, in the portions of the record where BIT values of >0.3 are observed, $U^{k'}_{37}$ SST estimates indicate relatively close agreement with those based on TEX_{86}, suggesting that soil organic matter input has not affected TEX_{86}-based SST estimates to a large degree. Thus, together $U^{k'}_{37}$ and TEX_{86} provide a robust SST record from the EM of the last 27 cal ka.

[21] A major feature of the BIT record is a large decrease in BIT values observed at ~9.5 cal ka (Figure 4). Although this may mistakenly be interpreted as a decrease in soil organic matter input to the EM, which is contrary to the hypothesis that increased runoff from the Nile River contributed to EM sapropel formation [e.g., *Rossignol-Strick et al.*, 1982], it should be noted that a major (order of magnitude) increase in the abundance of crenarchaeol occurs at this time (Figure 5). Following sapropel S1 (S1) deposition, abundances of crenarchaeol are significantly higher throughout the remainder of the Holocene compared to the Late Pleistocene. Therefore, the large decrease in BIT index values that occurs at ~9.5 cal ka can be attributed to a major increase in the abundance of crenarchaeol, accompanied by increased preservation. This illustrates the importance of quantifying abundances of GDGTs and examining this data in conjunction with BIT index values. Furthermore, it should be noted that during times of increased flow of the Nile River, inputs of total sediment to the Nile Delta actually decrease, as a consequence of increased vegetation cover in the Ethiopian highlands resulting from northward migrations of the Intertropical Convergence Zone [*Krom et al.*, 2002]. Thus, enhanced input of the Nile river, as suspected during sapropel formation, do not necessarily need to be accompanied by substantially higher soil input and increased BIT index values. We hypothesize that with the onset of the modern flow regime of the Nile River in the early Holocene [*Talbot et al.*, 2000], increased nutrient supply caused the increase in crenarchaeol, which was particularly elevated during S1 deposition.

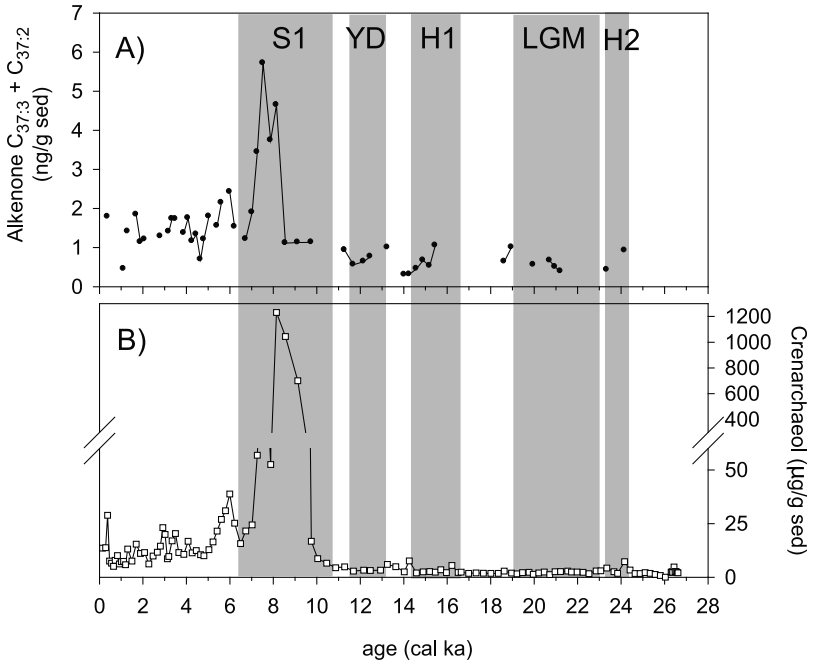

Figure 5. Abundances of alkenones and crenarchaeol in core GeoB 7702-3. The intervals of Heinrich event 2 (H2), the Last Glacial Maximum (LGM), Heinrich event 1 (H1), the Younger Dryas (YD), and sapropel S1 (S1) are highlighted. (a) The total sum of the $C_{37:3}$ and $C_{37:2}$ alkenones (ng/g sediment). (b) Total abundance of crenarchaeol (μg/g sediment). Note the scale break and the order of magnitude increase in abundance associated with the S1 sapropel.

[22] Another interesting observation is that in portions of our SST records, in particular at the terminations of Heinrich event 1 (H1) and the Younger Dryas (YD), changes observed in the TEX_{86}-based SST record appear to slightly lead changes in the $U^{k'}_{37}$ SST record (Figure 4). This may result from differences in preservation during lateral transport between GDGTs and alkenones. It has been observed in sediments that radiocarbon ages of crenarchaeol are relatively younger than those of alkenones, suggesting that alkenones are more prone to be affected by lateral transport compared to GDGTs [*Mollenhauer et al.*, 2007, 2008]. Additionally, *Kim et al.* [2009a] provide evidence that TEX_{86} is primarily influenced by local conditions and is less subject to long-distance lateral transport compared to the $U^{k'}_{37}$ index.

4.2. Thermal History of the EM

4.2.1. Heinrich Event 2

[23] In the central and western Mediterranean, significant SST cooling is noted during Heinrich event 2 (H2) [*Cacho et al.*, 1999, 2001; *Sierro et al.*, 2005]. The effects of H2 on the EM are less clear since relatively few paleoclimate records are of sufficient resolution to capture this event. In the $U^{k'}_{37}$ record of MD84-632 (Figure 1), the coolest interval of the past 30 cal ka occurs during H2 [*Essallami et al.*, 2007]. In GeoB 7702-3, alkenones are absent from this interval and cooling is not reflected in the TEX_{86} record (Figure 4). However, sediments older than 24 cal ka are characterized by high BIT values and thus TEX_{86} values may be influenced by soil organic matter input in this portion of the core.

4.2.2. Last Glacial Maximum

[24] In the TEX_{86} record, the LGM is characterized by SSTs ranging from 15°C to 17°C in the interval from 19 to 23 cal ka, similar to the few available $U^{k'}_{37}$ measurements (Figure 4). The lowest TEX_{86} value is noted at ~21.5 cal ka followed by a trend to increasingly warmer temperatures until 19.9 cal ka. From the end of the LGM until ~16.6 cal ka, the TEX_{86} record indicates an overall warming trend with brief cooling events at ~19.7 and 18.6 cal ka, and especially pronounced warming is observed before the H1 event (Figure 6). Early warming following the LGM previously has been reported from the EM [*Essallami et al.*, 2007] and from East African lake records [*Powers et al.*, 2005; *Tierney et al.*, 2008]. However, the Alboran Sea $U^{k'}_{37}$ record does not indicate warming until after ~16 cal ka (Figure 6) [*Cacho et al.*, 1999], suggesting differing responses during the deglaciation between the western and eastern Mediterranean.

[25] In GeoB 7702-3, the SST difference between the LGM and modern temperatures is ~10°C, based on TEX_{86}. Other studies have reported an EM LGM cooling of 6°C–7°C compared to present-day SST based on alkenone and foraminiferal data [*Essallami et al.*, 2007], and 2°C based on foraminiferal artificial neural networks (ANN) [*Hayes et al.*, 2005]. We observe a significantly larger SST decrease in comparison with previous studies, which is likely attributed to the TEX_{86} record reflecting summer SSTs during the

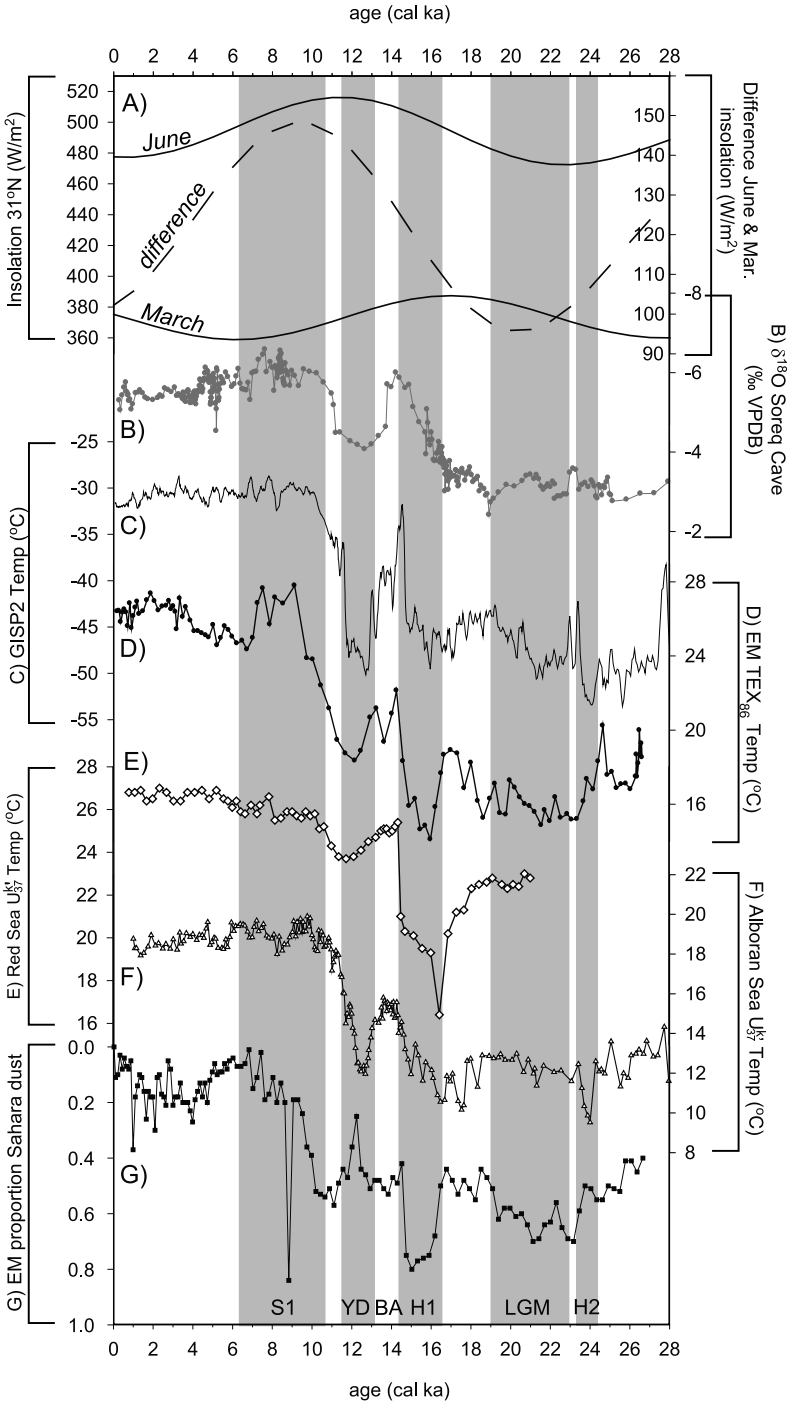

Figure 6. Comparison of climate records. The intervals of Heinrich event 2 (H2), the Last Glacial Maximum (LGM), Heinrich event 1 (H1), the Bølling-Allerød (BA), the Younger Dryas (YD), and sapropel S1 (S1) are indicated. Refer to Figure 1 for the location of paleoclimate records shown. (a) Spring (March) and summer (June) insolation at 31°N latitude [*Berger and Loutre*, 1991]. The difference between spring and summer insolation is indicated by the dashed line. (b) Oxygen isotope data from Soreq Cave in Israel [*Bar-Matthews et al.*, 1997, 1999, 2003]. (c) Temperature reconstruction from the GISP2 ice core in Greenland [*Alley*, 2004]. (d) TEX_{86} temperature record of GeoB 7702-3. (e) $U^{k'}_{37}$ SST estimates from core GeoB 5844-2 in the Red Sea [*Arz et al.*, 2003]. (f) $U^{k'}_{37}$ SST estimates from western Mediterranean core MD952043 [*Cacho et al.*, 2001]. (g) Eastern Mediterranean grain size data from *Hamann et al.* [2008]. The proportion of grain-size end-member 1 present in core GeoTu-SL112, which is attributed to dust influx from the Sahara, is plotted.

Holocene but not during the Pleistocene. The $U^{k'}_{37}$ SST difference between the youngest Holocene sediment containing alkenones at 0.37 cal ka and the LGM is ~8°C, in good agreement other EM $U^{k'}_{37}$ records [*Essallami et al.*, 2007]. Our SST records thus support the conclusions of *Essallami et al.* [2007], that the amplitude of the LGM SST cooling in the EM was >6°C, comparable to cooling observed in records from the central and western Mediterranean [*Cacho et al.*, 1999, 2001; *Hayes et al.*, 2005]. Therefore, paleoceanographic reconstructions based on a strong W-E SST gradient during the LGM likely need reconsideration [*Kuhlemann et al.*, 2008].

4.2.3. Heinrich Event 1

[26] The TEX_{86} record clearly reveals that H1 was a period of significant cooling in the EM (Figure 6d). This cooling initiated at ~16.6 cal ka, peaked at ~16.0 cal ka when a low temperature of ~14°C is observed, and terminated ~14.3 cal ka. In comparison to pre-H1 SSTs, an overall cooling of 4.5°C is noted. It is particularly notable that SSTs during H1 were at least 1°C cooler than during the LGM (Figure 6). A similar observation has been made for the Red Sea, where SSTs during H1 were 2°C cooler than LGM SSTs [*Arz et al.*, 2003]. The timing of the H1 event in GeoB 7702-3 agrees well with independently dated records from both the EM [*Hamann et al.*, 2008] (Figure 6g) and the Red Sea [*Arz et al.*, 2003] (Figure 6e). These records indicate that H1 started and ended abruptly in the EM region. In contrast to the EM and Red Sea records, in the Alboran Sea and the Atlantic side of the Iberian margin, such a well-defined excursion during the H1 event is not observed. In both the Alboran Sea [*Cacho et al.*, 2001] (Figure 6f) and Iberian Margin [*Martrat et al.*, 2007] $U^{k'}_{37}$ records, cooler SSTs are observed at the beginning of the H1 event (at ~16.5 cal ka) and subsequently, an overall warming trend occurs throughout the remainder of the H1 interval with warming continuing until ~14 cal ka. The differing responses of the western and eastern Mediterranean during H1 suggest that atmospheric teleconnections to the high latitudes may have contributed to H1 cooling in the EM region.

4.2.4. Bølling-Allerød and the Younger Dryas in the EM

[27] Following the H1 event, rapid warming is revealed by both the TEX_{86} and $U^{k'}_{37}$ records, with TEX_{86} SSTs of 19.4°C to 22.1°C and $U^{k'}_{37}$ SSTs of ~21°C noted in the interval from ~14.3 to 13.2 cal ka (Figure 4). This warming likely corresponds to the Bølling-Allerød (BA) warm period, and appears to be nearly synchronous with warming evident in the Greenland GISP2 ice core [*Alley*, 2004] (Figure 6c). *Essallami et al.* [2007] also note warmer $U^{k'}_{37}$ SSTs during the BA in the EM while in the Red Sea an abrupt temperature rise of 4.5°C occurs at the transition leading into the BA [*Arz et al.*, 2003] (Figure 6e).

[28] Following the BA, TEX_{86} and $U^{k'}_{37}$ records both indicate a return to cooler conditions, coincident in timing with the YD (Figure 4). TEX_{86} SSTs indicate a minimum temperature of ~18°C at 12.2 cal ka, while the $U^{k'}_{37}$ record indicates a minimum temperature of ~19°C at 11.6 cal ka. Between 13.2 and 12.2 cal ka a temperature decrease of ~3°C is noted in the TEX_{86} record and ~2°C in the $U^{k'}_{37}$ record, thereby demonstrating that the YD had a significant impact on EM SSTs. Cooling during the YD also is noted in the Red Sea [*Arz et al.*, 2003] and at Soreq Cave an excursion to more enriched $\delta^{18}O$ values occurs [*Bar-Matthews et al.*, 1997, 1999, 2003] (Figure 6).

[29] The differing responses of the EM region to high-latitude climate forcing during H1 and the YD is intriguing. In contrast to the rapid termination of H1, which is nearly synchronous between EM and high latitude records, during the termination of the YD the EM region experienced a delayed warming that was characterized by a more gradual transition into the Holocene than observed in high latitude records. This pattern is observed in our SST records, in the Red Sea SST record [*Arz et al.*, 2003], and in EM grain-size records [*Hamann et al.*, 2008] (Figures 1 and 5). Thus, it appears that while high-latitude forcing is a main driver of EM climate, other mechanisms exerted a greater influence on EM climate at times in the past. Modern atmospheric and wind patterns in the EM are influenced by equatorial and midlatitude climate forcings [*Kostopoulou and Jones*, 2007, and references therein]. However, increased equatorial forcing cannot explain the response of the EM during the YD because numerous records from equatorial Africa indicate an abrupt end to this event [e.g., *Johnson et al.*, 2002; *Castañeda et al.*, 2007; *Garcin et al.*, 2007; *Talbot et al.*, 2007; *Weldeab et al.*, 2007]. In the grain-size record of *Hamann et al.* [2008], the H1 event displays an abrupt start and termination with increased Saharan dust flux observed throughout the event. In contrast, during the YD Saharan dust supply was briefly reduced but increased by the end of the YD with increased inputs continuing into the early Holocene [*Hamann et al.*, 2008]. Increased dust influx to the EM, which likely derives from sources in eastern Libyan Desert, central Algeria, Egypt and Sudan [*Hamann et al.*, 2008], is noted until ~10 cal ka, suggesting that this region of the Sahara may have exerted a greater influence on EM climate at the end of the YD and into the early Holocene. We speculate that such a linkage may explain the observed delayed warming at the end of the YD.

4.2.5. Holocene Conditions in the EM

[30] The S1 sapropel layer, which is noted from ~9.7–7.0 cal ka in GeoB 7702-3, is marked by a significant increase in abundances of alkenones and crenarchaeol (Figure 5). Higher abundances of crenarchaeol and alkenones are generally noted throughout the Holocene in comparison to the period prior to ~10 cal ka (Figure 5), supporting the hypothesis that increased runoff of the Nile River, associated with the initiation of the African monsoon, is linked to increased nutrient supply and productivity in the EM [*Rossignol-Strick et al.*, 1982; *Calvert et al.*, 1992]. Following desiccation or closed basin conditions during the LGM and H1, the overflow of Lake Victoria, the source of the White Nile, was reestablished at ~14.5 cal ka [*Williams et al.*, 2006] while similarly, the overflow of Lake Tana, the source of the Blue Nile, was reestablished at ~14.8 cal ka [*Lamb et al.*, 2007]. After the YD, monsoonal conditions were established over much of tropical Africa, providing the central Sahara with regular rainfall [*Williams et al.*, 2006]. Thus, modern productivity patterns in the EM, including

seasonal differences in the timing of the crenarchaeota and haptophyte blooms, likely were established with the onset of the modern flow system of the Nile River.

[31] An interesting feature of our SST records is that significant warming is observed in the TEX_{86} record during S1 deposition (Figure 4). Between 9.7 and 9.1 cal ka, TEX_{86} SSTs increased by ~4°C while a decrease of ~2.7°C occurs between ~7.5 and 7.0 cal ka, at the termination of S1 deposition. Our observation of warmer TEX_{86}-based SSTs during sapropel deposition is opposite to a previous study of Pliocene sapropel layers, where cooling of TEX_{86} SSTs was observed in comparison to nonsapropel intervals [*Menzel et al.*, 2006]. It was hypothesized that in Pliocene sapropels, the decrease in TEX_{86} SSTs is due to shallowing of the chemocline during sapropel deposition, driving the crenarchaeota from the uppermost portion of the water column to nutrient-rich deeper waters around the chemocline, similar to the situation in present-day Black Sea [*Menzel et al.*, 2006]. However, there is not compelling evidence that the chemocline was located within the photic zone during S1 [*Coolen and Overmann*, 2007; *Sinninghe Damsté and Hopmans*, 2008] and thus the crenarchaeota may have not been driven to a different ecological niche in deeper waters. Our $U^{k'}_{37}$ SST record reveals no major excursions during S1 deposition (Figure 4), in agreement with the results of *Menzel et al.* [2006] who found no substantial differences in $U^{k'}_{37}$ SSTs between Pliocene sapropel and nonsapropel intervals. Conversely, *Emeis et al.* [2003] report warmer $U^{k'}_{37}$ SSTs in most Mediterranean sapropels.

[32] Another interesting feature of the TEX_{86} and $U^{k'}_{37}$ records is that during the Late Pleistocene SST estimates are similar between the two proxies, whereas the Holocene is characterized by elevated TEX_{86} SSTs in comparison to $U^{k'}_{37}$ SSTs (Figure 4). Thus, it appears that seasonal differences in the timing of the crenarchaeota and haptophyte blooms may have become more pronounced in the Holocene. Maximum Northern Hemisphere summer insolation occurs in the early Holocene [*Berger and Loutre*, 1991], and therefore, the exceptionally warmer TEX_{86} SSTs noted in comparison to the $U^{k'}_{37}$ SSTs may be partially attributed to warmer summers in the Early Holocene, or to the maximum difference between spring and summer insolation, which occurs at this time (Figure 6a). At present, average spring SSTs at the coring site are 17.25°C in March and 18.5°C in April, average summer SSTs are 26°C in July and 27.5°C in August and September, and average autumn SST is 26°C in October and 23.25°C in November [*Marullo et al.*, 1999]. Thus, significant differences exists between summer SST and either spring or fall SST in the modern situation. Likewise, a temperature difference of ~2.5°C is noted between TEX_{86} and $U^{k'}_{37}$ SST estimates in the youngest sediment samples. However, the increase in TEX_{86}-based SST in the S1 layer, of up to 5°C above $U^{k'}_{37}$ SST estimates, appears to be unusually high and the reasons for this are presently unclear although increased seasonality in the early Holocene is likely a contributing factor (Figure 6a). Large temperature differences of ~4°C are also observed between TEX_{86} and $U^{k'}_{37}$ SST estimates in the mid to late Holocene, particularly at around 2 cal ka. BIT index values remain below 0.3 throughout the entire Holocene (Figure 4) and thus TEX_{86}-based SSTs are unlikely to be influenced by input of soil organic matter. In the early Holocene, increased runoff from the Nile River is thought to have produced low-salinity surface waters and a strong density stratification, thereby causing bottom water anoxia [*van Straaten*, 1972; *Rossignol-Strick et al.*, 1982; *Nolet and Corliss*, 1990]. Previous studies of TEX_{86} in freshwater lakes [*Powers et al.*, 2004] and in mesocosm experiments [*Wuchter et al.*, 2004] have concluded that TEX_{86} values are not significantly affected by salinity. However, other factors such as light limitation and nutrient supply [*Prahl et al.*, 2006; *Versteegh et al.*, 2001] are known to influence the depth of alkenone production in the water column, as well as $U^{k'}_{37}$ values. It is likely that environmental factors other than SST may have influenced both the $U^{k'}_{37}$ and TEX_{86} records, contributing to the relatively large temperature differences observed between the two proxies during the Holocene.

[33] Following S1 deposition, the TEX_{86} SST record indicates generally increasing temperatures from 24.3°C at 6.7 cal to 27.4°C at 1.9 cal ka (Figure 6). Subsequently, a minor decrease in SST of <1°C is noted until the present. $U^{k'}_{37}$ SSTs range from a low value of 22.3°C at 6.2 cal ka to a high value of 25.6°C at 4.4 cal ka (Figure 4), although the record is quite variable and lacks any clear trends. In comparison to Late Pleistocene conditions, both the TEX_{86} and $U^{k'}_{37}$ records indicate relatively stable conditions during the Holocene. Generally stable Holocene conditions are also noted in the Red Sea [*Arz et al.*, 2003], the western Mediterranean [*Cacho et al.*, 2001], and in the EM record of *Essallami et al.* [2007] whereas the EM record of *Emeis et al.* [2000] displays greater variability but is of lower resolution.

5. Conclusions

[34] TEX_{86} and $U^{k'}_{37}$ analyses of core GeoB 7702-3 have revealed important information regarding the SST history of the EM region. By applying these two SST proxies to the same sediment samples, important insights regarding past seasonal influences on the SST proxies have been obtained. Our records show that Heinrich event 1, the Bølling-Allerød and the Younger Dryas all had major impacts on EM SST. The cooling noted during H1 was particularly severe, with SST being at least 1°C cooler than during the LGM. The transition from cool conditions during H1 to the Bølling-Allerød warm interval matches closely with the timing noted in Greenland ice core records. However, in contrast to Greenland ice core records, the transition from the Younger Dryas into the Holocene was not an abrupt event in the EM but occurred gradually over a period of ~2,000 years or more. At the start of the Holocene, an offset is observed between the $U^{k'}_{37}$ and TEX_{86} records, with the TEX_{86} record indicating warmer temperatures. This offset is likely due to seasonal differences in the timing of the haptophyte and crenarchaeota blooms in the EM, with the haptophyte bloom occurring in winter/early spring and the crenarchaeota bloom likely occurring in summer. This seasonal difference

was likely caused by the different nutrient regime that established when the modern flow system of the Nile River initiated at the start of the Holocene.

[35] **Acknowledgments.** We thank Marianne Baas, Ellen Hopmans, Jort Ossebaar, and Michiel Kienhuis for analytical assistance. Research funding was provided by NEBROC-2. Samples from GeoB 7702-3 were supplied through the assistance of the University of Bremen, Geosciences Department and MARUM. This work was supported by the DFG–Research Center/Excellence Cluster "The Ocean in the Earth System." We thank Gerald Dickens and two anonymous reviewers for comments that improved this manuscript.

References

Adamson, D. A., F. Gasse, F. A. Street, and M. A. J. Williams (1980), Late Quaternary history of the Nile, *Nature*, *288*, 50–55, doi:10.1038/288050a0.

Alley, R. B. (2004), GISP2 ice core temperature and accumulation data, http://www.ncdc.noaa.gov/paleo/metadata/noaa-icecore-2475.html, World Data Cent. for Paleoclimatology, Boulder, Colo.

Arz, H. W., J. Pätzold, P. J. Müller, and M. O. Moammar (2003), Influence of Northern Hemisphere climate and global sea level rise on the restricted Red Sea marine environment during termination I, *Paleoceanography*, *18* (2), 1053, doi:10.1029/2002PA000864.

Bar-Matthews, M., A. Ayalon, and A. Kaufman (1997), Late Quaternary paleoclimate in the eastern Mediterranean region from stable isotope analysis of speleothems at Soreq Cave, Israel, *Quat. Res.*, *47*, 155–168, doi:10.1006/qres.1997.1883.

Bar-Matthews, M., A. Ayalon, A. Kaufman, and G. J. Wasserburg (1999), The eastern Mediterranean paleoclimate as a reflection of regional events: Soreq Cave, Israel, *Earth Planet. Sci. Lett.*, *166*, 85–95, doi:10.1016/S0012-821X(98)00275-1.

Bar-Matthews, M., A. Ayalon, M. Gilmour, A. Matthews, and C. J. Hawkesworth (2003), Sea-land oxygen isotopic relationships from planktonic foraminifera and speleothems in the eastern Mediterranean region and their implication for paleorainfall during interglacial intervals, *Geochim. Cosmochim. Acta*, *67*, 3181–3199, doi:10.1016/S0016-7037(02)01031-1.

Berger, A., and M. F. Loutre (1991), Insolation values for the climate of the last 10 million years, *Quat. Sci. Rev.*, *10*, 297–317, doi:10.1016/0277-3791(91)90033-Q.

Brassell, S. C., G. Eglinton, I. T. Marlowe, U. Pflaumann, and M. Sarnthein (1986), Molecular stratigraphy: A new tool for climatic assessment, *Nature*, *320*, 129–133, doi:10.1038/320129a0.

Brasseur, P., J. M. Beckers, J. M. Brankart, and R. Schoenauen (1996), Seasonal temperature and salinity fields in the Mediterranean Sea: Climatological analyses of a historical data set, *Deep Sea Res., Part I*, *43*, 159–192, doi:10.1016/0967-0637(96)00012-X.

Cacho, I., J. O. Grimalt, C. Pelejero, M. Canals, F. J. Sierro, J. A. Flores, and N. Shackleton (1999), Dansgaard-Oeschger and Heinrich event imprints in Alboran Sea paleotemperatures, *Paleoceanography*, *14*, 698–705.

Cacho, I., J. O. Grimalt, M. Canals, L. Sbaffi, N. J. Shackleton, J. Schönfeld, and R. Zahn (2001), Variability of the western Mediterranean Sea surface temperature during the last 25,000 years and its connection with the Northern Hemisphere climatic changes, *Paleoceanography*, *16*, 40–52, doi:10.1029/2000PA000502.

Calvert, S. E., B. Nielsen, and M. R. Fontugne (1992), Evidence from nitrogen isotope ratios for enhanced productivity during formation of eastern Mediterranean sapropels, *Nature*, *359*, 223–225, doi:10.1038/359223a0.

Castañeda, I. S., J. P. Werne, and T. C. Johnson (2007), Wet and arid phases in the southeast African tropics since the Last Glacial Maximum, *Geology*, *35*, 823–826, doi:10.1130/G23916A.1.

Conte, M. H., M.-A. Sicre, C. Rühlemann, J. C. Weber, S. Schulte, D. Schulz-Bull, and T. Blanz (2006), Global temperature calibration of the alkenone unsaturation index ($U^{k'}_{37}$) in surface waters and comparison with surface sediments, *Geochem. Geophys. Geosyst.*, *7*, Q02005, doi:10.1029/2005GC001054.

Coolen, M. J. L., and J. Overmann (2007), 217 000-year-old DNA sequences of green sulfur bacteria in Mediterranean sapropels and their implications for the reconstruction of the paleoenvironment, *Environ. Microbiol.*, *9*, 238–249, doi:10.1111/j.1462-2920.2006.01134.x.

Emeis, K.-C., U. Struck, H.-M. Schulz, R. Rosenberg, S. Bernasconi, H. Erlenkeuser, T. Sakamoto, and F. Martinez-Ruiz (2000), Temperature and salinity variations of Mediterranean Sea surface waters over the last 16,000 years from records of planktonic stable oxygen isotopes and alkenone unsaturation ratios, *Palaeogeogr. Palaeoclimatol. Palaeoecol.*, *158*, 259–280.

Emeis, K.-C., et al. (2003), Eastern Mediterranean surface water temperatures and $\delta^{18}O$ composition during deposition of sapropels in the Late Quaternary, *Paleoceanography*, *18*(1), 1005, doi:10.1029/2000PA000617.

Essallami, L., M. A. Sicre, N. Kallel, L. Labeyrie, and G. Siani (2007), Hydrological changes in the Mediterranean Sea over the last 30,000 years, *Geochem. Geophys. Geosyst.*, *8*, Q07002, doi:10.1029/2007GC001587.

Fairbanks, R. G., R. A. Mortlock, T.-C. Chiu, L. Cao, A. Kaplan, T. P. Guilderson, T. W. Fairbanks, A. L. Bloom, P. M. Grootes, and M.-J. Nadeau (2005), Marine radiocarbon calibration curve spanning 0 to 50,000 years BP based on paired $^{230}Th/^{234}U/^{238}U$ and ^{14}C dates on pristine corals, *Quat. Sci. Rev.*, *24*, 1781–1796, doi:10.1016/j.quascirev.2005.04.007.

Ferguson, J. E., G. M. Henderson, M. Kucera, and R. E. M. Rickaby (2008), Systematic change of foraminiferal Mg/Ca ratios across a strong salinity gradient, *Earth Planet. Sci. Lett.*, *265*, 153–166, doi:10.1016/j.epsl.2007.10.011.

Garcin, Y., A. Vincens, D. Williamson, G. Buchet, and J. Guiot (2007), Abrupt resumption of the African monsoon at the Younger Dryas–Holocene climatic transition, *Quat. Sci. Rev.*, *26*, 690–704, doi:10.1016/j.quascirev.2006.10.014.

Goudie, A. S., and N. J. Middleton (2001), Saharan dust storms: Nature and consequences, *Earth Sci. Rev.*, *56*, 179–204, doi:10.1016/S0012-8252(01)00067-8.

Guerzoni, S., et al. (1999), The role of atmospheric deposition in the biogeochemistry of the Mediterranean Sea, *Prog. Oceanogr.*, *44*, 147–190, doi:10.1016/S0079-6611(99)00024-5.

Hamann, Y., W. Ehrmann, G. Schmiedl, S. Krüger, J. B. Stuut, and T. Kuhnt (2008), Sedimentation processes in the eastern Mediterranean Sea during the Late Glacial and Holocene revealed by end-member modelling of the terrigenous fraction in marine sediments, *Mar. Geol.*, *248*, 97–114, doi:10.1016/j.margeo.2007.10.009.

Hayes, A., M. Kucera, N. Kallel, L. Sbaffi, and E. J. Rohling (2005), Glacial Mediterranean Sea surface temperatures based on planktonic foraminiferal assemblages, *Quat. Sci. Rev.*, *24*, 999–1016, doi:10.1016/j.quascirev.2004.02.018.

Hopmans, E. C., S. Schouten, R. D. Pancost, M. T. J. van der Meer, and J. S. Sinninghe Damsté (2000), Analysis of intact tetraether lipids in archaeal cell material and sediments by high performance liquid chromatography/atmospheric pressure chemical ionization mass spectrometry, *Rapid Commun. Mass Spectrom.*, *14*, 585–589, doi:10.1002/(SICI)1097-0231(20000415)14:7<585::AID-RCM913>3.0.CO;2-N.

Hopmans, E. C., J. W. H. Weijers, E. Schefuß, L. Herfort, J. S. Sinninghe Damsté, and S. Schouten (2004), A novel proxy for terrestrial organic matter in sediments based on branched and isoprenoid tetraether lipids, *Earth Planet. Sci. Lett.*, *224*, 107–116, doi:10.1016/j.epsl.2004.05.012.

Hughen, K. A., et al. (2004), Marine04 marine radiocarbon age calibration, 0–26 cal kyr BP, *Radiocarbon*, *46*, 1059–1086.

Huguet, C., J.-H. Kim, J. S. Sinninghe Damsté, and S. Schouten (2006), Reconstruction of sea surface temperature variations in the Arabian Sea over the last 23 kyr using organic proxies (TEX_{86} and $U^{k'}_{37}$), *Paleoceanography*, *21*, PA3003, doi:10.1029/2005PA001215.

Johnson, T. C., E. T. Brown, J. McManus, S. Barry, P. Barker, and F. Gasse (2002), A high-resolution paleoclimate record spanning the past 25,000 years in southern East Africa, *Science*, *296*, 113–132, doi:10.1126/science.1070057.

Kim, J.-H., S. Schouten, E. C. Hopmans, B. Donner, and J. S. Sinninghe Damsté (2008), Global sediment core-top calibration of the TEX_{86} paleothermometer in the ocean, *Geochim. Cosmochim. Acta*, *72*, 1154–1173, doi:10.1016/j.gca.2007.12.010.

Kim, J.-H., X. Crosta, E. Michel, S. Schouten, J. Duprat, and J. S. Sinninghe Damsté (2009a), Impact of lateral transport on organic proxies in the Southern Ocean, *Quat. Res.*, *71*, 246–250, doi:10.1016/j.yqres.2008.10.005.

Kim, J.-H., C. Huguet, K. A. F. Zonneveld, G. J. M. Versteegh, W. Roeder, J. S. Sinninghe Damsté, and S. Schouten (2009b), An experimental field study to test the stability of lipids used for the TEX_{86} and $U^{k'}_{37}$ palaeothermometers, *Geochim. Cosmochim. Acta*, *73*, 2888–2898, doi:10.1016/j.gca.2009.02.030.

Kisakürek, B., A. Eisenhauer, F. Böhm, D. Garbe-Schönberg, and J. Erez (2008), Controls on shell Mg/Ca and Sr/Ca in cultured planktonic foraminiferan, *Globigerinoides ruber* (white), *Earth Planet. Sci. Lett.*, *273*, 260–269, doi:10.1016/j.epsl.2008.06.026.

Kostopoulou, E., and P. D. Jones (2007), Comprehensive analysis of the climate variability in the eastern Mediterranean. Part I: Map-pattern classification, *Int. J. Climatol.*, *27*, 1189–1214, doi:10.1002/joc.1467.

Krom, M. D., J. D. Stanley, R. A. Cliff, and J. C. Woodward (2002), Nile River sediment fluctuations over the past 7000 yr and their key role in sapropel development, *Geology*, *30*, 71–74, doi:10.1130/0091-7613(2002)030<0071:NRSFOT>2.0.CO;2.

Krom, M. D., S. Groom, and T. Zohary (2003), The eastern Mediterranean, in *The Biogeochemistry of Marine Systems*, edited by K. D. Black and G. B. Shimmield, pp. 91–122, Blackwell, Oxford, U. K.

Kubilay, N., S. Nickovic, C. Moulin, and F. Dulac (2000), An illustration of the transport and deposition of mineral dust onto the eastern Mediterranean, *Atmos. Environ.*, *34*, 1293–1303, doi:10.1016/S1352-2310(99)00179-X.

Kuhlemann, J., E. J. Rohling, I. Krumrei, P. Kubik, S. Ivy-Ochs, and M. Kucera (2008), Regional synthesis of Mediterranean atmospheric circulation during the Last Glacial Maximum, *Science*, *321*, 1338–1340, doi:10.1126/science.1157638.

Lamb, H. F., C. R. Bates, P. V. Coombes, M. H. Marshall, M. Umer, S. J. Davies, and E. Dejen (2007), Late Pleistocene desiccation of Lake Tana, source of the Blue Nile, *Quat. Sci. Rev.*, *26*, 287–299.

Lea, D. W., T. A. Mashiotta, and H. J. Spero (1999), Controls on magnesium and strontium uptake in planktonic foraminifera determined by live culturing, *Geochim. Cosmochim. Acta*, *63*, 2369–2379, doi:10.1016/S0016-7037(99)00197-0.

Lee, K. Y., J.-H. Kim, I. Wilke, P. Helmke, and S. Schouten (2008), A study of the alkenone, TEX_{86}, and planktonic foraminifera in the Benguela upwelling system: Implications for past sea surface temperature estimates, *Geochem. Geophys. Geosyst.*, *9*, Q10019, doi:10.1029/2008GC002056.

Martrat, B., J. O. Grimalt, N. J. Shackleton, L. de Abreu, M. A. Hutterli, and T. F. Stocker (2007), Four climate cycles of recurring deep and surface water destabilizations on the Iberian margin, *Science*, *317*, 502–507.

Marullo, S., R. Santoleri, P. Malanotte-Rizzoli, and A. Bergamasco (1999), The sea surface temperature field in the eastern Mediterranean from advanced very high resolution radiometer (AVHRR) data: Part 1. Seasonal variability, *J. Mar. Syst.*, *20*, 63–81, doi:10.1016/S0924-7963(98)00071-2.

Menzel, D., E. C. Hopmans, S. Schouten, and J. S. Sinninghe Damsté (2006), Membrane tetraether lipids of planktonic Crenarchaeota in Pliocene sapropels of the eastern Mediterranean Sea, *Palaeogeogr. Palaeoclimatol. Palaeoecol.*, *239*, 1–15, doi:10.1016/j.palaeo.2006.01.002.

Mollenhauer, G., M. Inthorn, T. Vogt, M. Zabel, J. S. Sinninghe Damsté, and T. I. Eglinton (2007), Aging of marine organic matter during cross-shelf lateral transport in the Benguela upwelling system revealed by compound-specific radiocarbon dating, *Geochem. Geophys. Geosyst.*, *8*, Q09004, doi:10.1029/2007GC001603.

Mollenhauer, G., T. I. Eglinton, E. C. Hopmans, and J. S. Sinninghe Damsté (2008), A radiocarbon-based assessment of the preservation characteristics of crenarchaeol and alkenones from continental margin sediments, *Org. Geochem.*, *39*, 1039–1045, doi:10.1016/j.orggeochem.2008.02.006.

Murray, A. E., A. Blakis, R. Massana, S. Strawzewski, U. Passow, A. Alldredge, and E. F. DeLong (1999), A time series assessment of planktonic archaeal variability in the Santa Barbara Channel, *Aquat. Microb. Ecol.*, *20*, 129–145, doi:10.3354/ame020129.

Nolet, G. J., and B. H. Corliss (1990), Benthic foraminiferal evidence for reduced deep-water circulation during sapropel deposition in the eastern Mediterranean, *Mar. Geol.*, *94*, 109–130, doi:10.1016/0025-3227(90)90106-T.

Nürnberg, D., J. Bijma, and C. Hemleben (1996), Assessing the reliability of magnesium in foraminiferal calcite as a proxy for water mass temperatures, *Geochim. Cosmochim. Acta*, *60*, 803–814, doi:10.1016/0016-7037(95)00446-7.

Pätzold, J., G. Bohrmann, and C. Hübscher (2003), Black Sea–Mediterranean–Red Sea: Cruise No. 52, *Meteor-Ber. 03-2*, 179 pp., Univ. Hamburg, Hamburg, Germany, 2 Jan. to 27 March.

Powers, L. A., J. P. Werne, T. C. Johnson, E. C. Hopmans, J. S. Sinninghe Damsté, and S. Schouten (2004), Crenarchaeotal membrane lipids in lake sediments: A new paleotemperature proxy for continental paleoclimate reconstruction?, *Geology*, *32*, 613–616, doi:10.1130/G20434.1.

Powers, L. A., T. C. Johnson, J. P. Werne, I. S. Castañeda, E. C. Hopmans, J. S. Sinninghe Damsté, and S. Schouten (2005), Large temperature variability in the southern African tropics since the Last Glacial Maximum, *Geophys. Res. Lett.*, *32*, L08706, doi:10.1029/2004GL022014.

Prahl, F. G., L. A. Muehlhausen, and D. L. Zahnle (1988), Further evaluation of long-chain alkenones as indicators of paleoceanographic conditions, *Geochim. Cosmochim. Acta*, *52*, 2303–2310, doi:10.1016/0016-7037(88)90132-9.

Prahl, F. G., A. C. Mix, and M. A. Sparrow (2006), Alkenone paleothermometry: Biological lessons from marine sediment records off western South America, *Geochim. Cosmochim. Acta*, *70*, 101–117, doi:10.1016/j.gca.2005.08.023.

Rossignol-Strick, M., W. Nesteroff, P. Olive, and C. Vergnaud-Grazzini (1982), After the deluge: Mediterranean stagnation and sapropel formation, *Nature*, *295*, 105–110, doi:10.1038/295105a0.

Schilman, B., A. Almogi-Labin, M. Bar-Matthews, L. Labeyrie, M. Paterne, and B. Luz (2001), Long- and short-term carbon fluctuations in the eastern Mediterranean during the late Holocene, *Geology*, *29*, 1099–1102, doi:10.1130/0091-7613(2001)029<1099:LASTCF>2.0.CO;2.

Schilman, B., A. Almogi-Labin, M. Bar-Matthews, and B. Luz (2003), Late Holocene productivity and hydrographic variability in the eastern Mediterranean inferred from benthic foraminiferal stable isotopes, *Paleoceanography*, *18*(3), 1064, doi:10.1029/2002PA000813.

Schouten, S., E. C. Hopmans, E. Schefuß, and J. S. Sinninghe Damsté (2002), Distributional variations in marine crenarchaeotal membrane lipids: A new tool for reconstructing ancient sea water temperatures?, *Earth Planet. Sci. Lett.*, *204*, 265–274, doi:10.1016/S0012-821X(02)00979-2.

Schouten, S., C. Huguet, E. C. Hopmans, M. V. M. Kienhuis, and J. S. Sinninghe Damsté (2007), Analytical methodology for TEX_{86} paleothermometry by high-performance liquid chromatography/atmospheric pressure chemical ionization-mass spectrometry, *Anal. Chem.*, *79*, 2940–2944, doi:10.1021/ac062339v.

Shah, S. R., G. Mollenhauer, N. Ohkouchi, T. I. Eglinton, and A. Pearson (2008), Origins of archaeal tetraether lipids in sediments: Insights from radiocarbon analysis, *Geochim. Cosmochim. Acta*, *72*, 4577–4594, doi:10.1016/j.gca.2008.06.021.

Sierro, F. J., et al. (2005), Impact of iceberg melting on Mediterranean thermohaline circulation during Heinrich events, *Paleoceanography*, *20*, PA2019, doi:10.1029/2004PA001051.

Sinninghe Damsté, J. S., and E. C. Hopmans (2008), Does fossil pigment and DNA data from Mediterranean sediments invalidate the use of green sulfur bacterial pigments and their diagenetic derivatives as proxies for the assessment of past photic zone euxinia?, *Environ. Microbiol.*, *10*, 1392–1399, doi:10.1111/j.1462-2920.2008.01609.x.

Stuiver, M., and P. J. Reimer (1993), Extended ^{14}C data base and revised Calib 3.0 ^{14}C age calibration program, *Radiocarbon*, *35*, 215–230.

Talbot, M. R., M. A. J. Williams, and D. A. Adamson (2000), Strontium isotope evidence for late Pleistocene reestablishment of an integrated Nile drainage network, *Geology*, *28*, 343–346, doi:10.1130/0091-7613(2000)28<343:SIEFLP>2.0.CO;2.

Talbot, M. R., M. L. Filippi, N. B. Jensen, and J.-J. Tiercelin (2007), An abrupt change in the African monsoon at the end of the Younger Dryas, *Geochem. Geophys. Geosyst.*, *8*, Q03005, doi:10.1029/2006GC001465.

Ternois, Y., M. A. Sicre, A. Boireau, M. H. Conte, and G. Eglinton (1997), Evaluation of long-chain alkenones as paleo-temperature indicators in the Mediterranean Sea, *Deep Sea Res., Part I*, *44*, 271–286, doi:10.1016/S0967-0637(97)89915-3.

Tierney, J. E., J. M. Russell, Y. S. Huang, J. S. Sinninghe Damsté, E. C. Hopmans, and A. S. Cohen (2008), Northern Hemisphere controls on tropical southeast African climate during the past 60,000 years, *Science*, *322*, 252–255, doi:10.1126/science.1160485.

van Straaten, L. M. J. U. (1972), Holocene stages of oxygen depletion in deep waters of the Adriatic Sea, in *The Mediterranean Sea*, edited by D. J. Stanley, pp. 631–643, Dowden Hutchinson Ross, Stroudsburg, Pa.

Versteegh, G. J. M., R. Riegman, J. W. de Leeuw, and J. H. F. Jansen (2001), $U^{k'}_{37}$ values for *Isochrysis galbana* as a function of culture temperature, light intensity and nutrient concentrations, *Org. Geochem.*, *32*, 785–794, doi:10.1016/S0146-6380(01)00041-9.

Wadie, W. F. (1984), The effect of regulation of the Nile River discharge on the oceanographic conditions and productivity of the southeastern part of the Mediterranean Sea, *Acta Adriat.*, *25*, 29–43.

Weijers, J. W. H., S. Schouten, O. C. Spaargaren, and J. S. Sinninghe Damsté (2006), Occurrence and distribution of tetraether membrane lipids in soils: Implications for the use of the TEX_{86}

proxy and the BIT index, *Org. Geochem.*, *37*, 1680–1693, doi:10.1016/j.orggeochem.2006.07.018.

Weldeab, S., K.-C. Emeis, C. Hemleben, and W. Siebel (2002), Provenance of lithogenic surface sediments and path ways of riverine suspended matters in the eastern Mediterranean Sea: Evidence from $^{143}Nd/^{144}Nd$ and $^{87}Sr/^{86}Sr$ ratios, *Chem. Geol.*, *186*, 139–149, doi:10.1016/S0009-2541(01)00415-6.

Weldeab, S., D. W. Lea, R. R. Schneider, and N. Andersen (2007), 155,000 years of West African monsoon and ocean thermal evolution, *Science*, *316*, 1303–1307, doi:10.1126/science.1140461.

Williams, M., M. Talbot, P. Aharon, Y. A. Salaam, F. Williams, and K. I. Brendeland (2006), Abrupt return of the summer monsoon 15,000 years ago: New supporting evidence from the lower White Nile valley and Lake Albert, *Quat. Sci. Rev.*, *25*, 2651–2665, doi:10.1016/j.quascirev.2005.07.019.

Wuchter, C., S. Schouten, M. J. L. Coolen, and J. S. Sinninghe Damsté (2004), Temperature-dependent variation in the distribution of tetraether membrane lipids of marine Crenarchaeota: Implications for TEX_{86} paleothermometry, *Paleoceanography*, *19*, PA4028, doi:10.1029/2004PA001041.

Wuchter, C., S. Schouten, S. G. Wakeham, and J. S. Sinninghe Damsté (2005), Temporal and spatial variation in tetraether membrane lipids of marine Crenarchaeota in particulate organic matter: Implications for TEX_{86} paleothermometry, *Paleoceanography*, *20*, PA3013, doi:10.1029/2004PA001110.

Ziveri, P., A. Rutten, D. J. de Lange, J. Thomson, and C. Corselli (2000), Present-day coccolith fluxes recorded in central eastern Mediterranean sediment traps and surface sediments, *Palaeogeogr. Palaeoclimatol. Palaeoecol.*, *158*, 175–195, doi:10.1016/S0031-0182(00)00049-3.

I. S. Castañeda, S. Schouten, and J. S. Sinninghe Damsté, Department of Marine Organic Biogeochemistry, Royal Netherlands Institute for Sea Research, PO Box 59, NL-1790 AB Den Burg, Texel, Netherlands. (isla.castaneda@nioz.nl)

J. Pätzold, Faculty of Geosciences, University of Bremen, Klagenfurter Straße, D-28359 Bremen, Germany.

E. Schefuß, MARUM, University of Bremen, Leobener Strasse, D-28359 Bremen, Germany.

S. Weldeab, Department of Earth Science, University of California, Santa Barbara, CA 93106-9630, USA.